Int J Adv Manuf Technol (2015) 79:793–803
DOI 10.1007/s00170-015-6842-7

ORIGINAL ARTICLE

Investigation of forming limit diagram for tube hydroforming considering effect of changing strain path

Lianfa Yang · Guolin Hu · Jianwei Liu

Received: 6 June 2014 / Accepted: 27 January 2015 / Published online: 18 February 2015

Abstract The forming limit diagram (FLD) has been widely used as a measure of the maximum formability of a material in tube hydroforming (THF). The geometric shape of the FLD varies owing to the influences of many factors, especially the strain path. Therefore, discussing the change rule of FLDs under various strain paths has practical significance. In the present study, strain paths generated from THF are classified as simple or complex ones. The FLDs for THF are established based on Swift's diffused necking criterion and Hill's localised necking criterion along both simple and complex strain paths. Through a comparison of the FLDs obtained from various strain paths, the influences of changing strain path are revealed. Some THF experiments under various strain paths are performed to verify the theoretical analysis. The theoretical analysis and experimental results prove that the position of the FLD changes with different strain paths. Compared with the FLD position established along a simple strain path, the FLD position under a two-stage linear strain path moves in the upper left direction with an initial uniaxial tensile strain path and in the lower right direction with an initial equibiaxial tensile strain path.

Keywords Tube hydroforming · Forming limit diagram (FLD) · Strain path · Necking criterion

Nomenclature

P_i/MPa	Instantaneous internal pressure (Figs. 1, 6b and 10)
δ_i/mm	Instantaneous tube wall thickness (Figs. 1 and 6b. 1) (Formula 4)
σ_1/MPa	Circumferential stress (Fig. 1) (Formula 3) (Formula 4)
σ_2/MPa	Longitudinal stress (Fig. 1) (Formula 3) (Formula 4)
ρ_1/mm	Instantaneous circumferential radius (Fig. 1) (Formula 4) (Formula 9)
ρ_2/mm	Instantaneous longitudinal radius (Fig. 1) (Formula 4) (Formula 9)
P_{max}/MPa	Maximum internal pressure (Fig. 2)
t_{max}/s	Maximum loading time (Fig. 2)
P_I/MPa	Internal pressure in initial stage (Fig. 2)
t_I/s	Loading time in initial stage (Fig. 2)
ε_1[—]	Circumferential strain (Fig. 4)
ε_2[—]	Longitudinal strain (Fig. 4)
β[—]	Strain ratio (Fig. 4) (Formula 7)
ρ_0/mm	Initial tube radius (Fig. 6a, b and Table 2)
δ_0/mm	Initial tube wall thickness (Fig. 6a) (Formula 4) (Table 2)
w/mm	Bugling length (Figs. 6 and 10)
r_d/mm	Die profile radius (Fig. 6)
$P0$/MPa	Initial internal pressure (Fig. 6a)
β_I[—]	Strain ratio of initial stage (Fig. 7)
β_{II}[—]	Strain ratio of subsequent stage (Fig. 7)
ε_{I1}[—]	Circumferential strain of initial stage under complex strain path (Fig. 8) (Formula 13)
ε_{I2}[—]	Longitudinal strain of initial stage under complex strain path (Fig. 8) (Formula 13)
ε_{II1}[—]	Circumferential strain of initial stage transformed into subsequent stage under complex strain path (Fig. 8) (Formula 13)
ε_{II2}[—]	Longitudinal strain of initial stage transformed into subsequent stage under complex strain path (Fig. 8) (Formula 13)
ε_{II3}[—]	Radial strain of subsequent stage under complex strain path (Formula 14)
γ_{xy}	Shearing strain (Fig. 8)
γ[—]	Rotation angle of principal strain axis (Fig. 8)

L. Yang (✉) · G. Hu · J. Liu
Faculty of Mechanical & Electrical Engineering, Guilin University of Electronic Technology, Guilin 541-004, Guangxi, People's Republic of China
e-mail: 27874113@qq.com

L_0/mm	Initial tube length (Fig. 7 and Table 2)
ε_3[—]	Radial strain (Formula 8)
$\overline{\sigma}$/MPa	Equivalent stress (Formula 10) (Formula 11)
$\overline{\varepsilon}$[—]	Equivalent strain (Formula 10) (Formula 12)
K/MPa	Strength coefficient (Formula 10) (Table 2)
n[—]	Strain hardening exponent (Formula 10) (Table 2)
σ_s/MPa	Yield strength (Formula 3) (Table 2)
σ_b/MPa	Tensile yield strength (Table 2)
ε_{II1}^*[—]	Circumferential strain of subsequent stage under complex strain path (Formula 15) (Formula 17)
ε_{II2}^*[—]	Longitudinal strain of subsequent stage under complex strain path (Formula 16) (Formula 18)
ε_1*[—]	Circumferential strain under complex strain path (Formula 19) (Formula 21)
ε_2*[—]	Longitudinal strain under complex strain path (Formula 20) (Formula 22)

1 Introduction

The tube hydroforming (THF) process is a type of near net shape technique that is used for producing tubular components in many fields including automobiles, aviation, aerospace, and household appliances. Compared with conventional metal-forming technologies such as stamping, THF offers tremendous advantages such as weight reduction, part consolidation, and improved dimensional tolerances.

The forming limit diagram (FLD) is conventionally described as a forming limit curve (FLC) in a plot of major strain ε_1 versus minor strain ε_2. It has been widely used as a measure of the maximum formability of a material in the THF process. If the maximum principal strain is above the FLC, it indicates that necking or fracture failure will occur; otherwise, failure will not occur and the process is safe. However, the geometric shapes of FLDs vary owing to the influences of many factors, especially the strain path. Therefore, discussing the change rule of FLDs under various strain paths has practical significance.

To investigate the influences of FLD for changing strain paths, FLDs under various strain paths should be established first. Plastic instability criteria are used as a limit strain criterion to calculate the maximum principal strain for establishing FLDs. At present, the plastic instability criteria are mainly of two types: macroscopic continuity instability criteria such as Swift's diffused necking criterion and Hill's localised necking criterion, and microcosmic damage mechanics instability criteria such as the M-K criterion that considers the plastic instability occurring on account of the microscopic defects accrued in the material. Some theoretical methods have been applied to study the FLD for THF. Kim [1] and Hwang [2] investigated the stresses and strains acting on an element at the middle of the tube and calculated the theoretical FLD for THF via Swift's diffused necking criterion and Hill's localised necking criterion along a simple strain path. Hashemi [3] established the FLD for THF along a simple strain path by using the M-K criterion. In addition to theoretical calculations, experimental methods can also be applied to establish the FLD for THF. Chen [4, 5] and Li [6] conducted forming limit experiments for THF and established the FLD for THF along a simple strain path. Most of these studies established the FLD along a simple strain path (one forming process); however, they did not study the effects of a changing strain path such as a complex strain path (multi-forming processes).

The present study aims to predict the FLDs for THF under two types of strain paths: simple strain paths and complex strain paths. Swift's diffused necking criterion and Hill's localised necking criterion are adopted as the failure criteria because in the M-K criterion, initial defects need to be set and have different correction forms. FLDs for THF along a simple strain path and a complex strain path are established via theoretical calculations. At the same time, forming limit experiments for THF are performed to establish the FLDs along a simple strain path and a complex strain path to verify the theoretical analysis. Through a comparison of these FLDs obtained from various strain paths, the influences of a changing strain path are revealed.

2 Classification of strain paths in THF processes

In this section, the strain paths generated from tube-free hydroforming processes are classified. The stresses and strains acting on an element at the middle of the tube are investigated to identify the type of strain path. The strain paths are closely related to the loading paths. The most common loading paths in tube-free hydroforming process are listed. The relationship between the strain paths and the loading paths is clarified. The strain paths during THF processes are classified as simple strain path and complex strain path. Any complex strain path can be transformed into broken-line strain paths combined with a number of linear strain paths by simplification. The classification of strain paths should help in establishing FLDs for THF under various strain paths.

Tube-free hydroforming means that a tubular blank is deformed just under the internal pressure. The stresses and strains acting on an element at the middle of the tube should be investigated to identify the type of strain path, as illustrated in Fig. 1. Assuming that the radial stress is zero during the tube-free hydroforming process, which implies that under plane stress condition, the main stress and strain directions are the circumferential and longitudinal directions of the tubular blank.

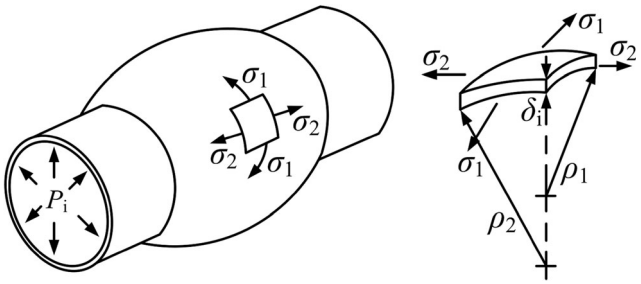

Fig. 1 Stresses acting on an element at the middle of the tube in free hydrobulging

The loading paths should be classified to identify the types of strain paths generated from tube-free hydroforming processes. A strain path is given by the ratio of the circumferential strain ε_1 constant to the longitudinal strain ε_2, which is closely related to the loading path. A loading path is given by the relationship between the internal pressure P and the loading time t. The strain paths show various forms depending on the different loading paths during tube-free hydroforming processes. The most common loading paths in tube-free hydroforming process are a linear loading path and a polygonal line loading path. The loading paths (pressure versus time) corresponding to the simple and complex strain paths used in theoretical calculation and experiments are shown in Fig. 2. The latter consists of two stages—the initial stage and the subsequent stage—the straight slopes of each of which are different. The internal pressure P_I is the maximum pressure in the initial stage, and the internal pressure P_{max} is the maximum pressure in the subsequent stage in the THF process. The strain path of an element at the middle of the tube is also linear under the condition of a linear loading path. The ratio of the circumferential strain ε_1 constant to the longitudinal strain ε_2 is essentially constant ($\beta=\varepsilon_2/\varepsilon_1$), and the principal axis of direction does not change. The strain path under a linear loading path is called a simple strain path. The values of β at

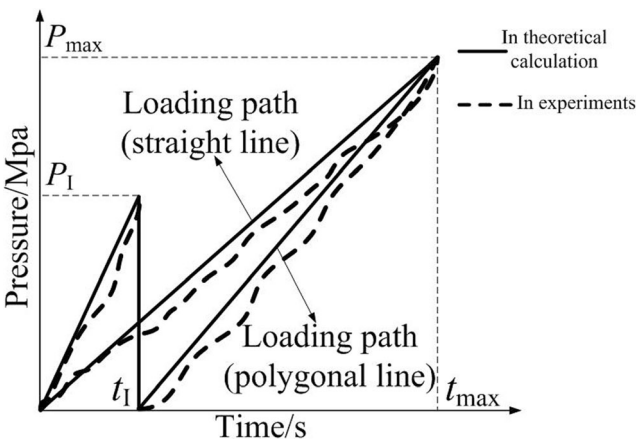

Fig. 2 The straight line loading paths and the polygonal line loading path adopted in theoretical calculation and experiments

various stages are different under a polygonal line loading path because the straight line slopes of each stage are different. The strain path of an element at the middle of the tube is nonlinear under a polygonal line loading path. The strain path under a polygonal line loading path is called a complex strain path. The strain path for some points from the start of experiment up to the tube failure in the case of complex strain paths are shown in Fig. 3. The above discussions suggest that the strain paths generated from tube-free hydroforming processes can be classified as simple strain paths and complex strain paths, as shown in Fig. 4. Any complex strain path can be transformed into broken-line strain paths combined with a number of linear strain paths by simplification. The classification of strain paths should help in establishing FLDs for THF under various strain paths.

3 Theoretical calculations to establish the FLD for THF under two types of strain paths by using the plastic instability criterion

In this section, the stresses and strains acting on an element at the middle of the tube are analysed and quantified. The plastic instability criterion adopted for calculating fracture strains under various strain paths is briefly introduced. Based on the force equilibrium equations and the relationship between the stress and the strain, the FLDs for THF under a simple strain path and a complex strain path are established by using the plastic instability criterion.

3.1 Brief introduction of plastic instability criterion

Tube-free hydroforming mainly fails at the axisymmetric position of the tube, which is called tensile failure along the circumferential direction. The plastic instability criterion can be used for judging whether the tube reaches fracture failure. In the present study, Swift's diffused necking criterion and Hill's localised necking criterion are used as the plastic instability criterion.

According to reference [7], the critical condition of plastic instability in Swift's diffused necking criterion can be expressed as

$$\frac{d\sigma_1}{\sigma_1} = d\varepsilon_1,\ \frac{d\sigma_2}{\sigma_2} = d\varepsilon_2 \tag{1}$$

The physical meaning of formula (1) is illustrated as follows: once the relative growth rate of tensile stress along the main stress direction attains the strain differential value, the moment is regarded as the onset of diffused necking at the potential fracturing position.

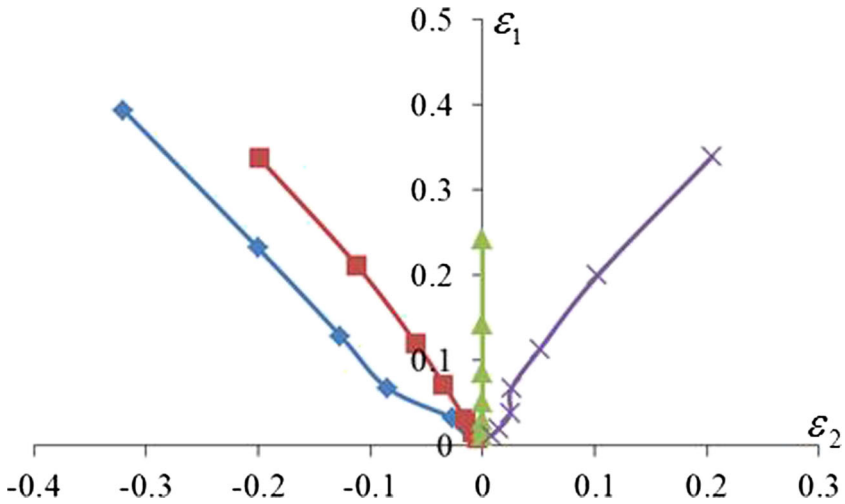

Fig. 3 The strain path for some points from the start of experiment up to the tube failure in the case of complex strain paths

According to reference [8], the critical condition of plastic instability in Hill's localised necking criterion can be expressed as

$$\frac{d\sigma_1}{\sigma_1} = -d\varepsilon_3,\ \frac{d\sigma_2}{\sigma_2} = -d\varepsilon_3 \tag{2}$$

The physical meaning of formula (2) is illustrated as follows: once the relative growth rate of tensile stress along the main stress direction attains the thickness reduction of the tube, the moment is regarded as the onset of localised necking or bursting at the potential fracturing position.

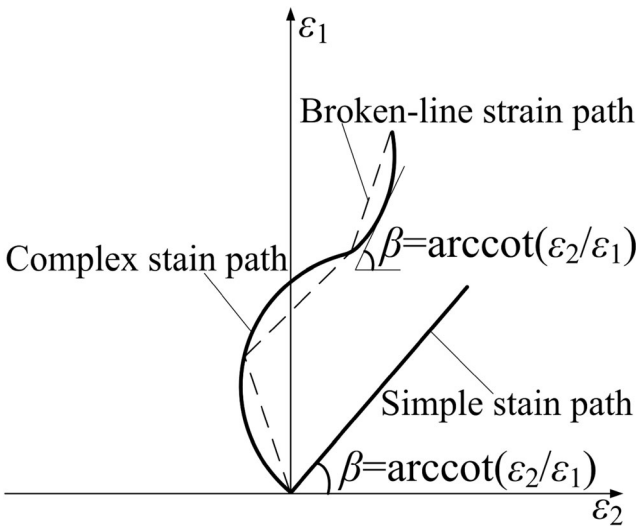

Fig. 4 Simple strain path and complex strain path (simplified by *broken-line strain paths*) generated from tube-free hydrobulging process

3.2 Theoretical calculation of the FLD for THF under simple strain path

The flow chart for the calculation of FLDs under simple and complex strain paths are illustrated in Fig. 5. Assume that the radial stress is zero during a tube-free hydroforming process, which implies the under plane stress condition, as illustrated in Fig. 1. The material is assumed to be isotropic, and the formula for the yield criterion during the THF process can be derived as

$$\sigma_1^2 - \sigma_1\sigma_2 + \sigma_2^2 = \sigma_s^2 \tag{3}$$

The following equilibrium equations of the stresses and strains acting on an element at the middle of the tube can be written as [9]

$$P_i = t_i\left(\frac{\sigma_1}{\rho_1} + \frac{\sigma_2}{\rho_2}\right) \tag{4}$$

$$\rho_1 = \rho_0 \exp\varepsilon_1,\ t_i = t_0 \exp\varepsilon_3 \tag{5}$$

$$\varepsilon_1 = \ln\rho_1/\rho_0,\ \varepsilon_3 = \ln t_i/t_0 \tag{6}$$

$$\beta = \varepsilon_2/\varepsilon_1 \tag{7}$$

The elastic deformation can be ignored relative to the plastic deformation during the THF process. The following expression can be written under constant volume:

$$\varepsilon_1 + \varepsilon_2 + \varepsilon_3 = 0 \tag{8}$$

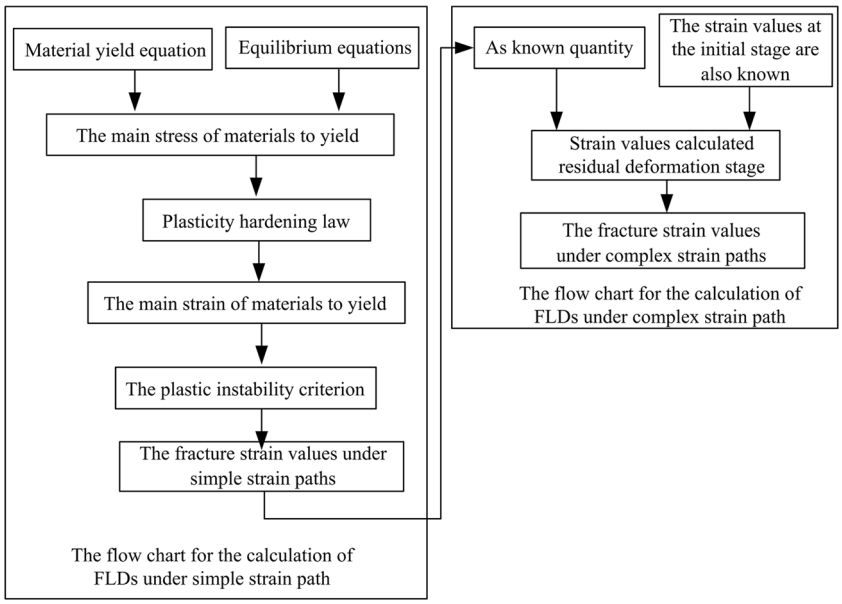

Fig. 5 The flow chart for the calculation of FLDs under simple and complex strain paths

To obtain the longitudinal radius ρ_2, the profile shape of the tube along the longitudinal direction during the THF processes is generally assumed as a straight line, which means longitudinal radius $\rho_2=\infty$, or as a sine curve, cosine curve, circle curve, or ellipse curve, which means longitudinal radius $\rho_2<\infty$ [10]. In the present study, an ellipse curve profile shape is assumed, as illustrated in Fig. 6. The elliptic function can be expressed as

$$\frac{x^2}{\rho_2^2}+\frac{y^2}{\rho_1^2}=1 \tag{9}$$

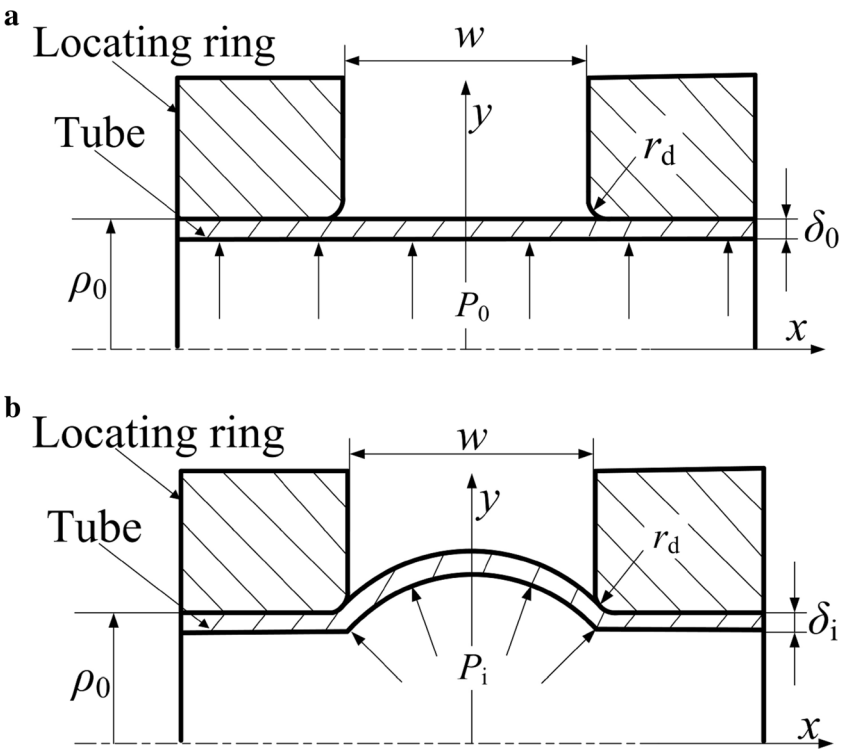

Fig. 6 Two states of tube-free hydroforming: **a** initial state and **b** intermediate state (assume ellipse curve profile shape along longitudinal direction during THF process)

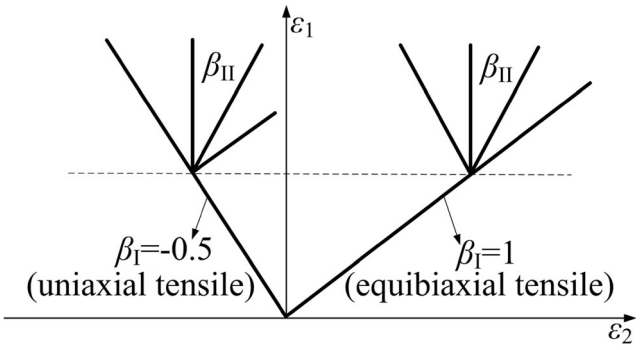

Fig. 7 Sketch of two typical initial strain paths in which the characteristic values are β_I=−0.5 and β_I=1 in the *broken-line strain paths*

We assume that the tube material obeys the Hollomon plasticity hardening law, which can be written as [4]

$$\overline{\sigma} = K\overline{\varepsilon}^{n} \tag{10}$$

The computational formula for equivalent stress and equivalent strain can be expressed as follows:

$$\overline{\sigma} = \sqrt{\frac{1}{2}\left[(\sigma_1-\sigma_2)^2 + \sigma_2^2 + \sigma_1^2\right]} \tag{11}$$

$$\overline{\varepsilon} = \sqrt{\frac{2}{9}\left[(\varepsilon_1-\varepsilon_2)^2 + (\varepsilon_2-\varepsilon_3)^2 + (\varepsilon_3-\varepsilon_1)^2\right]} \tag{12}$$

From the above discussions, the equation for formula (10) can be obtained. Then, using a mathematical iteration method, one can predict the FLD for THF under a simple strain path by solving a nonlinear equation combined with Swift's diffused necking criterion and Hill's localised necking criterion.

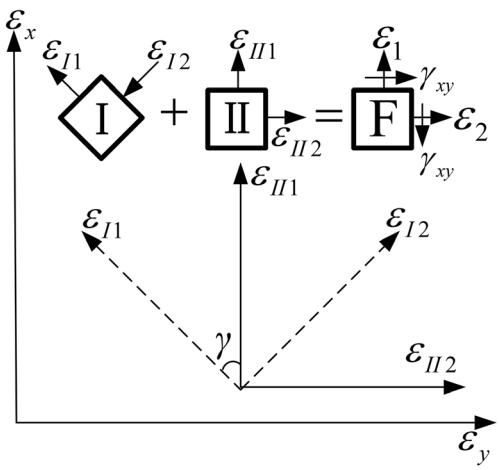

Fig. 8 Rotation γ of strain principal axis between the initial and the subsequent strain paths

Fig. 9 The CNC Tube Hydroforming system YB98-200A (made in China) was applied to conduct the hydroforming experiments

3.3 Theoretical calculation of the FLDs for THF under complex strain path

Any complex strain path can be transformed into broken-line strain paths combined with a number of linear strain paths by

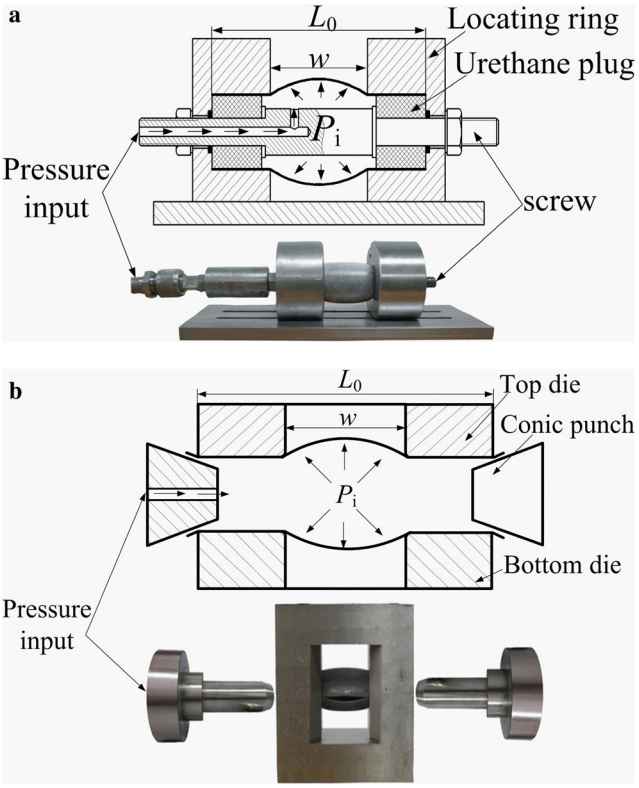

Fig. 10 Two-set experimental devices applied in the bulging experiments: **a** tube ends free one and **b** tube ends fixed one, which creates tension-compression and tension-tension strain state on the element at the middle of the tube, respectively

Table 1 Some test parameters with the conducted hydroforming experiments

	Simple strain path (FLD-1)			Initial uniaxial tensile strain path (FLD-2)		Initial equibiaxial tensile strain path (FLD-3)	
	Tube ends free		Tube ends fixed	Initial stage Tube ends free	Subsequent stage Tube ends free	Initial stage Tube ends fixed	Subsequent stage Tube ends fixed
Whether an axial movement of the tube ends was enabled or not	Axial movement		No axial movement	Axial movement	Axial movement	No axial movement	No axial movement
Bulging lengths/mm	48	96	48	48	96	48	48
Pressure/MPa	25.8	24.9	25.2	24.5	19.08	24.7	20.49

simplification, as shown in Fig. 2. Broken-line strain paths consist of two stages: initial stage and subsequent stage. The characteristic value of the strain path during these respective stages is β_{I} and β_{II}, as shown in Fig. 7. The strain paths of uniaxial tensile ($\beta_{\mathrm{I}}=-0.5$) and biaxial stretching ($\beta_{\mathrm{I}}=1$) are two typical stress and strain conditions that are used for establishing the FLDs under a complex strain path.

According to whether the strain principal axis between the initial and the subsequent strain paths is rotated, two cases should be focused upon under broken-line strain paths.

If the rotation of a strain principal axis is γ, as shown in Fig. 8, the formulae and its computing steps are given as follows:

(1) Assume that the fracture strain values in the circumferential, longitudinal, and radial directions under a simple strain path are known; then, the strain values for these three directions at the initial stage are also known.
(2) Assume that the direction of the radial strain can never be changed during the THF process and that the strain principal axis cannot be rotated.
(3) According to Fig. 8, the principal strain values under the initial stage can be transformed to those in the subsequent stage by using the following coordinate conversion formula [11]:

$$\begin{aligned} \varepsilon_{II1} &= \varepsilon_{I1} cos\gamma \\ \varepsilon_{II2} &= \varepsilon_{I2} cos\gamma \end{aligned} \tag{13}$$

(4) The surplus radial strain after the initial stage can be calculated as follows:

$$\varepsilon_{II3} = \varepsilon_3 - \varepsilon_{I3} \tag{14}$$

(5) According to the condition with constant volume, the principal strain values under the subsequent stage can be calculated as follows:

$$\varepsilon^*_{II_1} = \frac{\varepsilon_{II3}}{1+\beta_{II}} \tag{15}$$

$$\varepsilon^*_{II_2} = \beta_{II}\varepsilon_{II1} \tag{16}$$

The circumferential strain value obtained by solving formula (15) is negative, although it is positive in practice. Therefore, it is given by the absolute value of $\varepsilon_{\mathrm{II3}}$, and the principal strain values under the subsequent stage can be calculated as follows:

$$\varepsilon^*_{II_1} = \frac{|\varepsilon_{II3}|}{1+\beta_{II}} \tag{17}$$

$$\varepsilon^*_{II_2} = \beta_{II}\varepsilon_{II1} \tag{18}$$

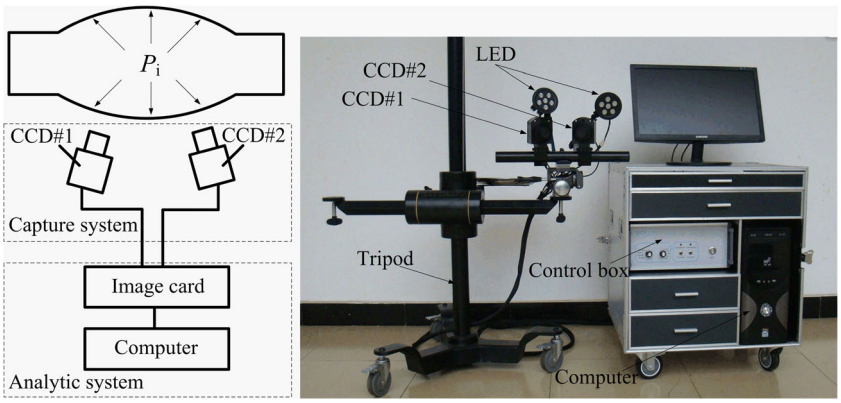

Fig. 11 Digital image correlation (DIC) measurement system of strain used to measure the speckle field online during tube hydrobulging experiments: schematic diagram (on the *left*) and photo show (on the *right*)

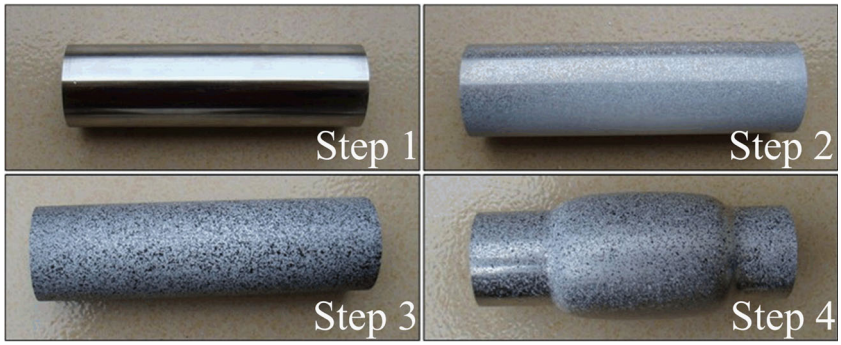

Fig. 12 Black and white spots sprayed on the tube surface used to form an initial speckle field

(6) From the above steps, the fracture strain values under any complex strain path can be calculated as follows:

$$\varepsilon_1^* = \varepsilon_{II_1}^* + \varepsilon_{II1} \tag{19}$$

$$\varepsilon_2^* = \varepsilon_{II_2}^* + \varepsilon_{II2} \tag{20}$$

If the strain principal axis is not rotated, this means that the strain principal axis under the initial and the subsequent stages overlap, the calculation formula can be simplified as follows:

$$\varepsilon_1^* = \varepsilon_{I1} + \varepsilon_{II_1}^* \tag{21}$$

$$\varepsilon_2^* = \varepsilon_{I2} + \varepsilon_{II_2}^* \tag{22}$$

4 Experimental methods to establish the FLDs for THF under two types of strain paths

In this section, forming limit experiments for THF are conducted under a simple and a complex strain path. In tube-free hydroforming, the fracture strain values under various strain paths can be measured by using an online strain mapping system.

The FLD is conventionally described as an FLC consisting of different limit state points. The FLC can be divided into two sides: in the left-hand side, the limit state is a tension-compression strain state, and in the right-hand side, the limit state is a tension-tension strain state. The limit states can be changed over the strain paths. Hence, through experimental methods, two problems need to be solved for establishing the FLD for THF under various strain paths. One is the formation of limit state, which means that an arbitrary point on the surface of the object can be used to attain the limit state. The other is the change in strain state, which can be called the change in strain path.

The experiments were performed on a CNC Tube Hydroforming system YB98-200A, made in China, as shown in Fig. 9. The built-in electric pressure testing pumps were used to control the hydraulic pressure. Two-set experimental devices for THF have been applied in the experiments—tube ends free and tube ends fixed bulging devices—as shown in Fig. 10. During tube hydrobulging, tube ends free is realised by allowing free shrinkage of a material in the axial direction, whereas tube ends fixed is realised by squeezing the tube ends into a trumpet shape and limiting axial shrinkage. In tube ends free bulging experiments, the circumferential strain of an element at the middle of the tube is tension strain and the longitudinal strain is compression strain. The limit states are matched to the left-hand side of the FLD. In tube ends fixed experiments, the circumferential strain of an element at the middle of the tube is tension strain and so is the longitudinal strain. The limit states are matched to the right-hand side of the FLD. To change the limit states, the bugling lengths of the tubular blank are different. The bugling lengths of the tubular blank are considered multiples of the tube diameter in the subsequent tube hydrobulging. The more details with the

Table 2 Mechanical properties and geometrical parameters of SS304 stainless steel

Material	Mechanical properties				Geometrical parameters			
	Elasticity modulus E/GPa	Tensile yield strength σ_b/MPa	Yield strength σ_s/MPa	Strength coefficient K/MPa	Hardening exponent n	Initial tube radius ρ_0/mm	Initial tube wall thickness δ_0/mm	Initial tube length L_0/mm
SS304	207	654	410	1623.31	0.43	16	0.75	150

conducted test parameters include some information about whether an axial movement of the tube ends was enabled or not, bulging lengths and pressure can be found in Table 1.

In the experiments, some of the tubes failed in the vicinity of the weld seam or parting line of tools, but some of the tubes failed in the area of a weld seam or parting line of tools, which would influence the measured values. Therefore, three tube specimens were used for each forming conditions and the forming data were collected on the specimen which failed in the area of a weld seam to improve the trustworthiness to the results.

In tube hydrobulging, the speckle field is measured by using a XJTUDIC digital image correlation (DIC) measurement system of strain, as shown in Fig. 11, which is developed by Xi'an Jiaotong University, China. The range of strain rate is from 0 to 50 as the change of deformation time. The online strain mapping system consists of a capture system and an analytic system, which can be used for online measurements of the strain values. In the capture system, two industrial cameras are used to capture the strain states during the bulging process. In the analytic system, the reference state (initial state of tube-free bulging) should be chosen first. The strain values can be calculated by comparing the strain state with the reference state.

For choosing the reference state, before the start of the experiment, black and white spots used to construct a speckle field should first be sprayed on the tube surface, as shown in Fig. 12. The position of the speckle field will move with the action of the internal pressure, and the strain values can be determined from the change in the speckle field.

Any complex strain path can be transformed into broken-line strain paths combined with a number of linear strain paths by simplification. In tube hydroforming processes with broken-line strain paths, the loading paths consist of two stages: in the initial stage, the tube is predeformed with the action of the initial internal pressure P_1, and in the subsequent stage, the tube attains the limit state with the action of the subsequent internal pressure P_{max}, as shown in Fig. 2. In the theoretical calculation, the initial strain paths are uniaxial tensile ($\beta_1=-0.5$) and biaxial stretching ($\beta_1=1$). For consistency with the theoretical calculation, two initial strain paths are adopted in the experiments for predeforming the tube. The prestress can be calculated through the following formula when predeforming the tube [4]:

$$P_i = \frac{\sigma_1 t_i}{\rho_1} \tag{23}$$

Tube ends free bulging devices can be used when the initial strain path is uniaxial tensile ($\beta_1=-0.5$), circumferential strain of an element at the middle of the tube is tension strain, and longitudinal strain is compression strain. Tube ends fixed bulging devices can be used when the initial strain path is biaxial stretching ($\beta_1=1$), circumferential strain of an element at the middle of the tube is tension strain, and longitudinal strain is also tension strain. After predeforming the tube, the bugling lengths of the tubular blank are different in order to change the limit states. The bugling lengths of the tubular blank are multiples of the tube diameter during subsequent tube hydrobulging.

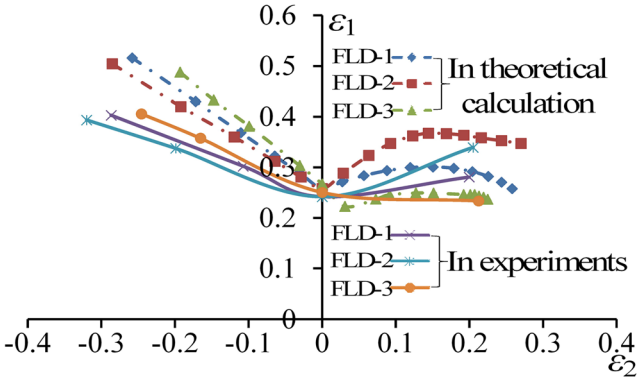

Fig. 13 FLDs under various strain paths obtained by theoretical calculation and THF experiments

5 Results and discussion

In this section, the FLDs for THF are established along simple and complex strain paths based on Swift's diffused necking criterion and Hill's localised necking criterion. Through a comparison of these FLDs obtained from various strain paths, the influences of changes in strain path are revealed. FLDs are obtained from THF experiments under various strain paths to verify the theoretical analysis.

5.1 FLDs under two types of strain paths obtained by theoretical calculation

In the present study, SS304 stainless steel is used as the tubular material; its mechanical properties and geometrical

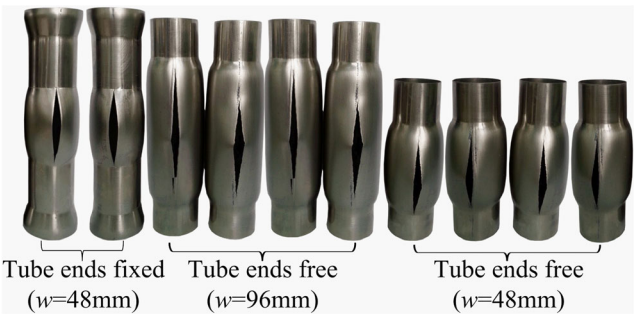

Fig. 14 Some hydroformed parts at different bulging lengths under various strain paths

parameters as shown in Table 2. The differential equation in formula (10) can be used to predict the FLD for THF by solving nonlinear equations and using the mathematical iteration method combined with the plastic instability criterion.

Assume zero rotation of the strain principal axis between the initial strain path and the subsequent strain path. Then, FLDs can be established by formulas (21) and (22) by setting the initial strain values. Assume that the initial strain path is under uniaxial tensile strain (β_1=−0.5) and that the initial equivalent strain value of an element at the middle of the tube is 0.095 (circumferential strain is 0.2, longitudinal strain is −0.1). Furthermore, assume that the initial strain path is under biaxial stretching (β_1=1) and that the initial equivalent strain value of an element at the middle of the tube is also 0.095 (circumferential strain is 0.1, longitudinal strain is 0.1). The FLDs for THF are established along simple and complex strain paths as shown in Fig. 13. Figure 13 shows that the FLD position drifts with a change in the strain paths. Compared with the FLD position established along a simple strain path (FLD-1), the FLD position under a two-stage linear strain path moves in the upper left direction with an initial uniaxial tensile strain path (FLD-2) and in the lower right direction with an initial equibiaxial tensile strain path (FLD-3). From Fig. 13, one may notice that in the plane strain state (ε_2=0), all FLCs are almost overlapped. In addition, the maximal differences between the predicted results and experimental data for FLD1, FLD2, and FLD3 are 5.3, 6.4, and 5.7 %, respectively.

5.2 FLDs obtained by THF experiments under two strain paths

The loading path is a straight line in THF experiments under a simple strain path. The fracture strains ε_1 and ε_2 when the tube fractured were used for establishing the FLD for THF under the simple strain path. The loading path is a polygonal line in THF experiments under a complex strain path, which consists of the initial and the subsequent strain path. In the initial stage, the prestress under the initial strain path for uniaxial tensile strain (β_1=−0.5) and biaxial stretching (β_1=1) can be calculated as 19.08 and 20.49 MPa, respectively, by formula (23) when predeforming the tube. In the subsequent stage, the hydroformed parts at different bulging lengths are shown in Fig. 14. The fracture strains ε_1 and ε_2 when the tube fractured were used for establishing the FLD for THF under a complex strain path.

The FLDs obtained by THF experiments are established along simple and complex strain paths as shown in Fig. 13. Figure 13 shows that the FLD position drifts with a change in the strain paths. The changing trend is consistent with that of FLDs obtained by theoretical calculations.

6 Conclusions

The strain paths generated from tube-free hydrobulging processes were classified as simple and complex strain paths. Any complex strain path can be transformed into broken-line strain paths combined with a number of linear strain paths by simplification. FLDs for THF under a simple and a complex strain path were established via Swift's diffused necking criterion and Hill's localised necking criterion. Forming limit experiments for THF were performed to establish the FLDs under a simple and a complex strain path to verify the result of theoretical analysis. Through a comparison of these FLDs obtained under various strain paths, the influences of changing strain path were revealed. The following conclusions were drawn from this study.

(1) The FLD position for THF drifts with a change in the strain paths.
(2) Compared with the FLD position established along a simple strain path (FLD-1), the FLD position moves in the upper left direction under a two-stage linear strain path with an initial uniaxial tensile strain path (FLD-2).
(3) Compared with the FLD position established along a simple strain path (FLD-1), the FLD position moves in the lower right direction under a two-stage linear strain path with an initial equibiaxial tensile strain path (FLD-3).

Acknowledgments The authors gratefully acknowledge the support of the National Natural Science Foundation of China (grant number 51065006&51271062), Guangxi Natural Science Foundation (grant number 2013GXNSFAA019305), and Guangxi Key Laboratory of Manufacturing System & Advanced Manufacturing Technology (grant number 11-031-12_006).

References

1. Jeong K, Sang-Woo K, Woo-Jin S, Beom-Soo K (2004) Analytical approach to bursting in tube hydroforming using diffuse plastic instability. Int J Mech Sci 46:1535–1547
2. Yeong-Maw H, Yi-Kai L, Han-Chieh C (2009) Forming limit diagrams of tubular materials by bulge tests. J Mater Process Technol 209:5024–5034
3. Ramin H, Ahmad A, Ehsan MKA (2009) Implementation of the forming limit stress diagram to obtain suitable load path in tube hydroforming considering M–K model. Mater Des 30:3545–3553
4. Xian-Feng C, Zhong-Qi Y, Bo H, Shu-Hui L, Zhong-Qin L (2011) A theoretical and experimental study on forming limit diagram for a seamed tube hydroforming. J Mater Process Technol 211:2012–2021
5. Xian-Feng C, Shu-Hui L, Zhong-Qi Y, Zhong-Qin L (2012) Study on experimental approaches of forming limit curve for tube hydroforming. Int J Adv Manuf Technol 61:87–100
6. Shu-Hui L, Xian-Feng C, Qing-Shuai K, Zhong-Qi Y, Zhong-Qin L (2012) Study on formability of tube hydroforming through elliptical die inserts. J Mater Process Technol 212:1916–1924
7. Swift HM (1952) Plastic instability under plane stress. J Mech Phys Solids 1:1–18

8. Hill R (1952) On discontinuous plastic states with special reference to localized necking in the sheet. J Mech Phys Solids 1:19–31
9. Woo-Jin S, Seong-Chan H, Tae-Wan K, Jeong K, Beom-Soo K (2010) Evaluation of effect of flow stress characteristics of tubular material on forming limit in tube hydroforming process. Int J Mach Tools Manuf 50:753–764
10. Yeong-Maw H, Yi-Kai L, Taylan A (2007) Evaluation of tubular materials by a hydraulic bulge test. Int J Mach Tools Manuf 47: 343–351
11. Francesco G, Giuseppe N, Giuseppe P, Alessandro S (2011) Simultaneous and integrated strain tensor estimation from geodetic and satellite deformation measurements to obtain three-dimensional displacement maps. IEEE Trans Geosci Remote Sens 49:1815–1826